

## Cover Page

Fill out and attach to your manuscript — DUE Monday, November 30, 2015

25th International Toki Conference (ITC-25)  
*Creating the Future*  
*- Innovative Science of Plasma and Fusion -*

Presentation Number:	P1-88
Paper Title:	Preliminary design of imaging bolometer fields of view for Wendelstein7-X
Corresponding Author:	Byron Jay Peterson
Affiliation:	National Institute for Fusion Science
Full Postal Address:	322-6 Toki, Gifu 509-5292, Japan
Telephone:	+81-572-58-2239
Fax:	+81-572-58-2624
E-mail:	peterson@LHD.nifs.ac.jp
Topic Category in ITC-25 (see the list below)	(1)
<b>LIST OF TOPICS CATEGORY in ITC-25</b> (1) Helical Plasma Research (2) Tokamak and ITER-related Research (3) Innovative Applications of Plasmas - Industrial/Chemical/Medical and Agricultural Applications - (4) Basic Plasma Science - Laboratory and Space Plasmas- (5) Fusion Technology Research (6) Theory and Simulation Research (7) Laser Plasma Sciences (8) Plasma Wall Interaction Research (9) Other Fields of Sciences <b>Notes:</b> ● <b>Above categories are not in one-to-one correspondence with the 6 topics in the submission site of PFR. Please choose a topic which is mostly related to your article when you submit a paper on PFR online submission site (PERAS).</b>	

## Preliminary design of imaging bolometer fields of view for Wendelstein7-X

Byron J. Peterson<sup>1,2</sup>, Kiyofumi Mukai<sup>1,2</sup>, Ryuichi Sano<sup>3</sup>, Haruki Kojima<sup>1</sup>, LHD Experiment Group<sup>1</sup>,  
Daihong Zhang<sup>4</sup>, Marcin Jakubowski<sup>4</sup>, Maciej Krychowiak<sup>4</sup>, Yuhe Feng<sup>4</sup>, Ralf Koenig<sup>4</sup>, Thomas  
Sunn Pedersen<sup>4</sup> and the W7-X Experiment Group<sup>4</sup>

<sup>1</sup>National Institute for Fusion Science, <sup>2</sup>SOKENDAI (The Graduate University for Advanced Studies),

<sup>3</sup>National Institutes for Quantum and Radiological Science and Technology, <sup>4</sup>Max Planck Institute for Plasma Physics

The InfraRed imaging Video Bolometer (IRVB) provides absolutely calibrated images of the plasma radiation. In this paper we present the design of four imaging bolometers viewing divertor and non divertor regions of Wendelstein7-X (W7-X). This design assumes a 640 x 480 pixel, 30 fps, 100 mK, IR camera imaging each IRVB foil. The bolometer cameras consist of a 9 cm x 7 cm x 2  $\mu$ m thick Pt foils blackened with graphite, which are located distances ranging 6 cm to 8 cm from a 4.3 mm x 4.3 mm aperture. The 8 cm x 6 cm central section of the foil is divided into 24 x 18 IRVB channels each consisting of 504 IR camera pixels. Using a previously derived expression, the noise equivalent power of the IRVB is calculated as 109  $\mu$ W/cm<sup>2</sup>. Assuming 5 MW of radiated power uniformly emanating from the 30 m<sup>3</sup> plasma, the signal level is estimated as ranging from 4.5 to 8.1 mW/cm<sup>2</sup> giving signal to noise ratios between 42 and 74.

Keywords: bolometer, diagnostics, imaging, divertor, Wendelstein7-X

### 1. Introduction

The InfraRed imaging Video Bolometer (IRVB) [1] measures plasma radiation images, which can be directly compared with the results of impurity radiation models to provide a quantitative measurement of the spatial distribution of the plasma radiation [2]. In a three-dimensional (3D) device such as Wendelstein7-X (W7X) [3, 4] the two-dimensional (2D) images provided by the IRVB are necessary to understand the complicated divertor and x-point radiation patterns. The ten-fold W7X divertor is divided into two sections, designated as the ‘low iota’ divertor and the ‘high iota’ divertor, referring to the magnetic configuration under which the divertor flux to those sections is dominant [5]. By observing the radiation from these two divertor sections, as well as non-divertor portions of the plasma, and comparing the bolometric images with synthetic images derived from impurity transport codes we plan to investigate impurity transport and confinement in W7-X.

In this paper we give information on the design of four IRVBs for W7-X. The ports utilized for this design are the AEM30 and AEA31 ports. The ports and divertor sections are shown in a computer aided drawing (CAD) in Figure 1. IRVB A views the ‘high iota’ divertor and IRVB B views the non divertor region, both from the AEM30 port. IRVB C views the ‘low iota’ divertor and IRVB D views the non divertor region, both from the AEA31 port. FoVs of both divertor and non divertor regions are planned in order to increase the coverage of

the 3D W7-X plasma as well as to differentiate between radiation resulting from the helical x-points and that resulting from plasma wall interaction at the divertor plate by comparing the experimental images with synthetic images from a 3D impurity transport model. Since the model may not include the radiation from plasma wall interactions, by comparing the synthetic image and the experimental image we should be able to differentiate between the two.

### 2. IRVB design parameters

The IRVB consist of two parts, the bolometer camera and the infrared (IR) camera, IR vacuum window and its associated optics as shown in Figure 2. The bolometer camera is based on a simple pinhole camera design with a

Table 1 IRVB design parameters

	$l_{ap-f}$	$S_{signal}$	SNR
IRVB	(cm)	(mW/cm <sup>2</sup> )	
A	7.5	5.2	47
B	6	8.1	74
C	8	4.5	42
D	7	5.9	54

9 cm x 7 cm x 2 micron thick Pt foil mounted in a frame and blackened with graphite viewing the plasma through a 4.3 mm x 4.3 mm square aperture. The distances from the foil to the aperture (shown in Figure 2),  $l_{ap-f}$ , vary depending on the IRVB and its field of view (FoV) and are given in Table 1. With regard to the IR camera and

optics, this design assumes a 640 x 480 pixel, 30 fps, 100 mK, microbolometer (8 - 12  $\mu\text{m}$ ) type IR camera imaging the IRVB foil. This design does not include any specification of the IR periscope which may be necessary to bring the IR signal out of the immersion tube to a location where sufficient space is available to install the

actual value of 50 mK in order to take into account any losses in the transmission through the periscope optics.

### 3. IRVB positions, FoVs and signal to noise ratios

The 8 cm x 6 cm central section of each foil is divided into 24 x 18 IRVB channels each consisting of

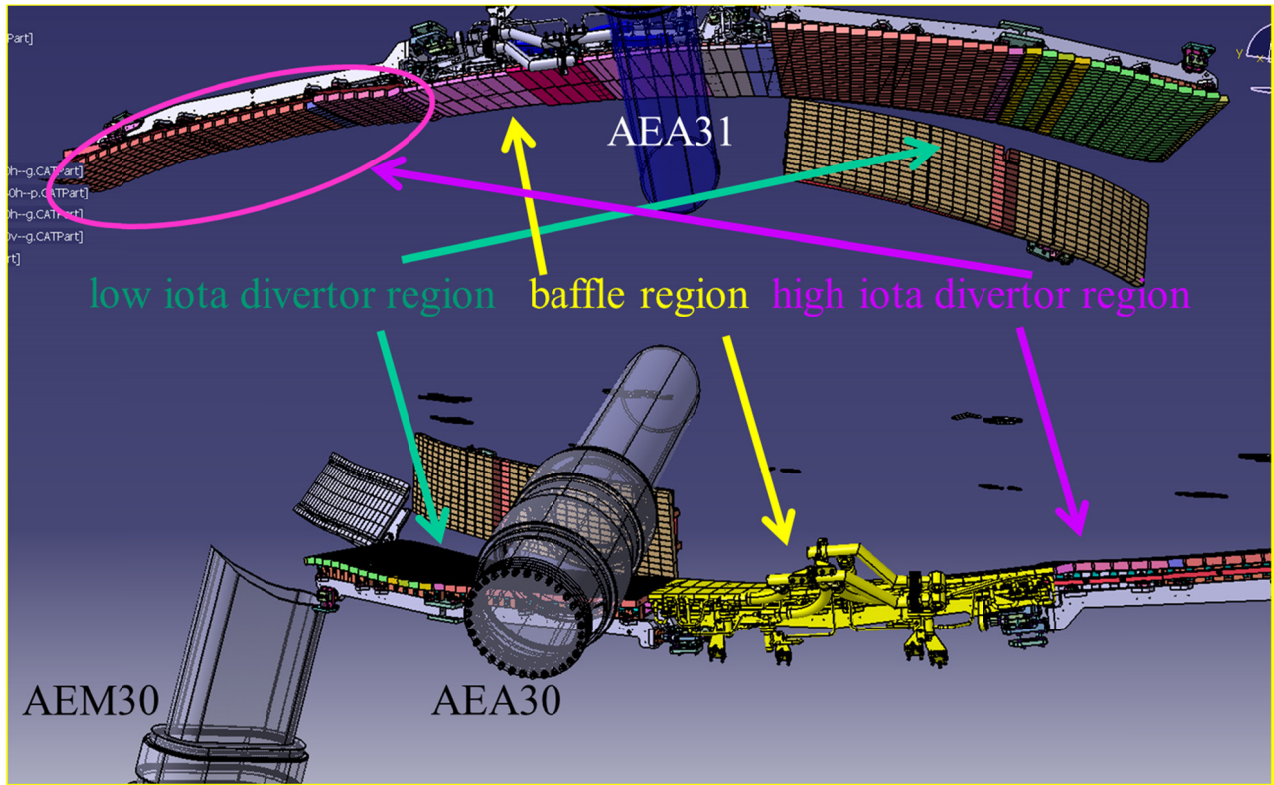


Fig. 1 CAD image of divertors and of ports used in W7-X for IRVBs.

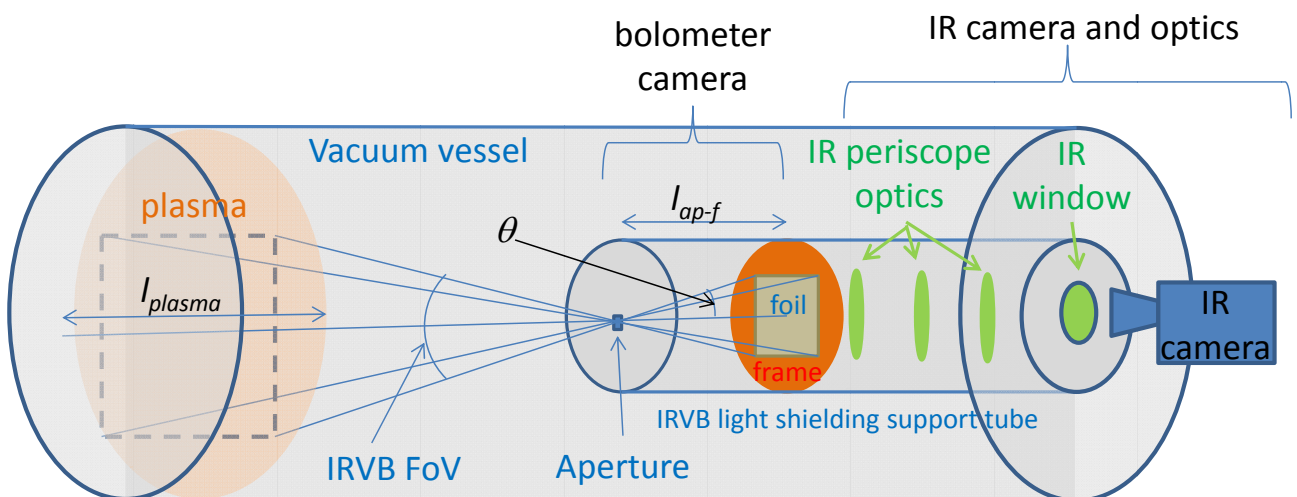


Fig. 2 Cartoon showing main components of IRVB.

IR camera and any shielding that may be necessary. The IR camera noise equivalent temperature (NET),  $\sigma_{IR}$ , is estimated conservatively to be 100 mK compared to the

504 IR camera pixels. The positions of the IRVB foils and apertures are given in Table 2. The coordinates are defined with respect to the center of the inside (vacuum

side) surface of the flange with  $x$  being in the toroidal direction (clockwise viewed from the top of the machine),  $y$  being in the negative poloidal direction (defined as positive being downward on the outboard side) and  $z$  being the distance from the inside (vacuum) surface of the flange with positive being towards the plasma. The coordinate systems are defined by the green axes in Figure 3. The coordinate system of the AEA31 port is rotated  $22.5^\circ$  clockwise (viewed from the atmosphere side towards the vacuum side) around the  $z$  axis in order to align the FoV of IRVB C with the low iota divertor.

The cross-section drawing of each port drawn through the

Table 2 IRVB coordinates

Port	IRVB	foil/ aperture	x (mm)	y (mm)	z (mm)
AEM 30	A	foil	0	175	1485
		aperture	-10	195	1560
	B	foil	0	-175	1380
		aperture	-20	-195	1440
AEA 31	C	foil	0	-50	1340
		aperture	22	-10	1420
	D	foil	0	50	1370
		aperture	-40	20	1440

vertical center of the foils is shown in Figure 3 and the FoVs of each IRVB channel are shown by the black grids in Figure 4.

The noise equivalent power density (NEPD),  $S_{IRVB}$ , of the IRVB is calculated using Equation 1

$$S_{IRVB} = \frac{\eta_{IRVB} N_{bol}}{A_f} = \frac{\sqrt{10kt_f\sigma_{IR}}}{\sqrt{f_{IR}N_{IR}}} \sqrt{\frac{N_{bol}^3 f_{bol}}{A_f^2} + \frac{N_{bol} f_{bol}^3}{5\kappa^2}} \quad (1)$$

where  $\eta_{IRVB}$  is the IRVB noise equivalent power density,  $N_{bol} = 432$  is the number of IRVB channels,  $A_f = 48 \text{ cm}^2$  is the utilized area of the foil,  $k = 0.716 \text{ W/cmK}$  is the thermal conductivity of the foil,  $t_f = 2 \text{ }\mu\text{m}$  is the thickness of the foil,  $f_{IR} = 30 \text{ fps}$  is the frame rate of the IR camera,  $N_{IR}$  is the number of IR camera pixels used,  $f_{bol} = 30 \text{ fps}$  is the frame rate of the IRVB and  $\kappa = 0.251 \text{ cm}^2/\text{s}$  is the foil thermal diffusivity. This equation is derived from Eq. 10 in Ref. [6] by dividing  $\eta_{IRVB}$  by the area of each bolometer channel,  $A_{bol} = A_f/N_{bol} = 11.1 \text{ mm}^2$  and neglecting the contribution of the black body radiation term. The first term under the radical is also small and can also be neglected, but we retain it in the calculations. Applying this equation to our design results in an  $S_{IRVB}$  of  $109 \text{ }\mu\text{W/cm}^2$ .

The signal level,  $S_{signal}$ , is simply calculated by assuming a uniformly radiating plasma using Eq. 2

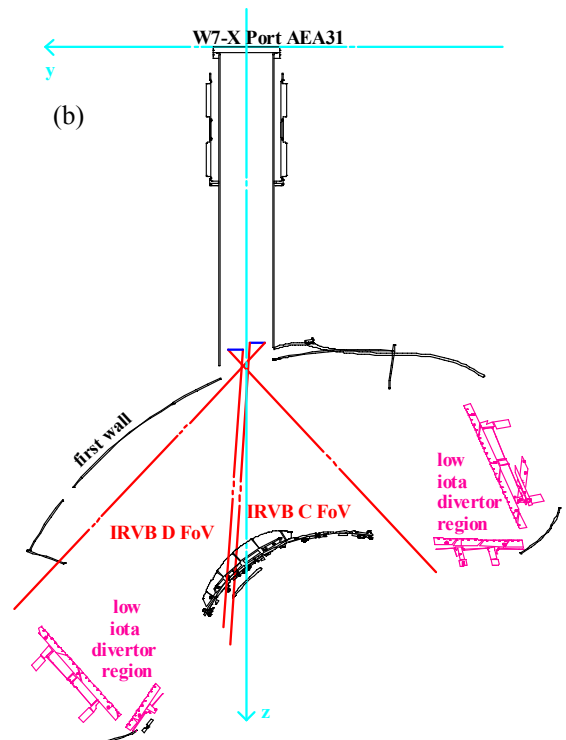
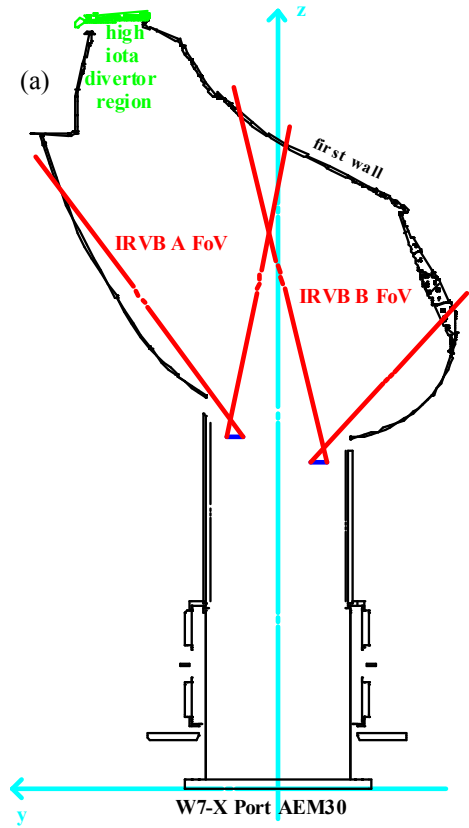


Fig. 3 CAD drawings of cross-sections of Ports AEM30 (a) and AEA31 (b) showing foil and aperture locations and the fields of view (red) of each IRVB.



$$S_{\text{signal}} = \frac{P_{\text{signal}}}{A_{\text{bol}}} = \frac{A_{\text{bol}} A_{\text{ap}} \cos^4 \theta P_{\text{rad}} l_{\text{plasma}}}{A_{\text{bol}} 4\pi l_{\text{ap-f}}^2 V_{\text{plasma}}} \quad (2)$$

where  $P_{\text{signal}}$  is the radiated power to each detector from the plasma,  $A_{\text{ap}} = 18.8 \text{ mm}^2$  is the area of the aperture,  $P_{\text{rad}} = 5 \text{ MW}$  is the total power radiated by the plasma,  $V_{\text{plasma}} = 30 \text{ m}^3$  is the volume of the plasma. The following three quantities are shown in Figure 2: the distance from the foil to the aperture,  $l_{\text{ap-f}}$ , the average path length of the sightline through the plasma,  $l_{\text{plasma}} = 150 \text{ cm}$ , and the average angle of each detector's line of sight with respect to the aperture normal vector,  $\theta = 20^\circ$ . Assuming these values, the signal level estimates and signal to noise ratios (SNR) given by the ratio of Eq. 1 to Eq. 2 are shown in Table 1. Using Equations 1 and 2 the bolometer pixels sizes and corresponding aperture sizes are chosen to give the maximum number of channels (and therefore best spatial resolution) while maintaining a reasonable SNR.

#### 4. Summary and future work

This work has shown that IRVBs with reasonable FoVs, numbers of channels and signal levels can be designed for W7-X. The main bolometer camera parameter,  $l_{\text{ap-f}}$ , and the locations of the foils and apertures given in Table 2 are chosen to give an adequate view of the respective divertor region for IRVBs A and C without being too close to the plasma. In the case of IRVBs B and D the locations of the apertures and foils and the selection of  $l_{\text{ap-f}}$  are somewhat arbitrary and will be optimized in the next step (see below).

The next step in the design process is to calculate the projection matrix for each IRVB and then multiply it by the radiated power density (resulting from an impurity transport code such as EMC3-EIRENE) to produce a synthetic image. These synthetic images will then provide a detailed estimate of the signal level for each channel that then can be used to provide a more accurate estimate of the SNR. Also the synthetic images can be used to fine tune the FoVs for IRVBs B and D which are viewing the non divertor regions.

#### Acknowledgement

This work was supported by NIFS budget code NIFS15ULHH026 and the NIFS International Collaboration budget.

#### 5. References

- [1] B. J. Peterson, Rev. Sci. Instrum. **71** (2000) 3696.

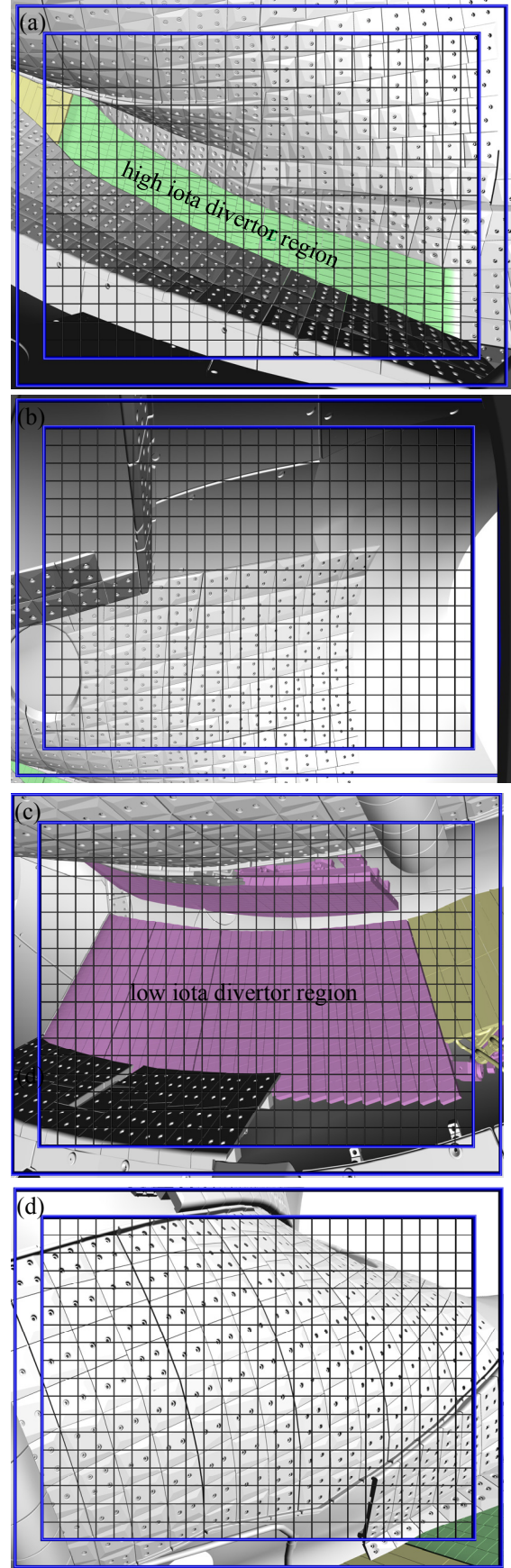


Fig. 4 CAD images of FoVs for IRVBs A (a), B (b), C (c) and D (d) in W7-X showing high (green), low (purple) iota divertor and baffle (yellow).

- [2] K. Mukai et al., Nucl. Fusion **55** (2015) 083016.
- [3] T. Klinger et al, Fus. Eng. Design **88** (2013) 461.
- [4] H. S. Bosch, et al., IEEE Trans. Plasma Sci. **42** (2014) 432.
- [5] H. Renner et al., J. Plasma Fusion Res. SERIES **1** (1998) 143.
- [6] B. J. Peterson, et al., Rev. Sci. Instrum. **74** (2003) 2040.